Mechanics of jet scour downstream of a headcut

Mécanisme de l'affouillement dû à un jet en aval d'une petite chute

O. R. STEIN
Department of Civil and Agricultural Engineering, Montana State University, Bozeman, MT, USA 59717

P. Y. JULIEN
Department of Civil Engineering, Colorado State University, Fort Collins, CO, USA 80523

C. V. ALONSO
USDA-ARS Hydro-Ecosystems Research Group, Fort Collins, CO, USA 80522

SUMMARY
Scour immediately downstream of a headcut is analyzed by considering the effect of jet diffusion on sediment detachment. The analytical development results in equations for:
1. the equilibrium scour depth;
2. the rate of scour hole development.
These equations are applicable for a variety of jet configurations and any bed material including cohesive soils. The equations are tested in laboratory simulated headcuts on bed materials consisting of two non-cohesive uniform sands and one cohesive natural soil. The agreement between measured and predicted rates of scour depth increase shows that scour does not increase as a semi-logarithmic function of time. The rate of scour depth increase is very rapid for depths less than 95% of the equilibrium scour depth. Graphical solutions for the rate of scour depth increase are in agreement with the experimental measurements.

RÉSUMÉ
Le mécanisme d'érosion immédiatement en aval d'une chute est analysé en considérant l'effet du jet sur l'arrachement des sédiments. Un système d'équations a été établi qui permet de calculer:
1. la profondeur d'affouillement à l'équilibre;
2. le développement dans le temps de la fosse d'affouillement.
Ces équations peuvent s'appliquer à une grande variété de configurations d'écoulement et de matériaux mobiles y compris les sols cohésifs. Les équations ont été calées sur des essais en laboratoire avec des matériaux mobiles consistant d'une part en un mélange de deux sables non cohésifs de granulométrie uniforme et d'autre part un sol naturel cohésif. La comparaison entre mesures et calculs montre que la profondeur d'affouillement n'évolue pas selon une loi semi-logarithmique en fonction du temps. L'accroissement de la profondeur d'affouillement est très rapide pour des profondeurs inférieurs à 95% de la valeur limite. Les solutions graphiques donnant l'acroissement de la profondeur d'affouillement sont en bon accord avec les valeurs expérimentales.

Revision received December 27, 1992. Open for discussion till June 30, 1994.

1 Introduction

Scour from impinging jets has long been a research focus because it is the driving mechanism causing scour below grade control structures and dam spillways. Most investigations have considered the equilibrium scour depth in non-cohesive bed material, equilibrium scour depth being reached when the sediment particles detached from the bed cannot leave the scour hole. Jet impingement also exerts the dominant erosive action on cohesive soil below headcuts in rills and gullies. Relatively little attention has been paid to this process, which is important in terms of soil erosion characteristics and dendritic drainage network evolution, as headcuts often define the upstream end of rills and gullies.

The primary objective of this study is to examine the scour caused by free overfall jets in small scale channels such as rills. The analysis stems from the theoretical investigation of jet diffusion characteristics in a plunge pool and the erosion characteristics of the impinging jet on both cohesive and non-cohesive particles. First, a theoretical description of jet diffusion, flow velocities, shear stresses and sediment detachment characteristics is presented. This theory is then compared to a laboratory data set. The data set focuses on the changes in scour profiles with time produced by a free falling nappe for both cohesive and non-cohesive material.

2 Diffusion of free overfall jets

The flow diagram shown in Fig. 1 illustrates a jet produced by a free falling nappe entering a plunge pool. The jet, with an origin at the water surface and initial thickness y_o, enters the plunge pool at an angle χ and nearly uniform average velocity U_o.

Free jets, unaffected by a boundary, spread laterally and diffuse throughout the surrounding fluid decreasing in average velocity, as analyzed by Albertson et al. (1950). The zone in which the centerline velocity remains constant at U_o defines the potential core, of length J_p from the jet origin. Beyond this distance, the velocity U remains a maximum along the jet centerline but the entire velocity field is reduced by diffusion.

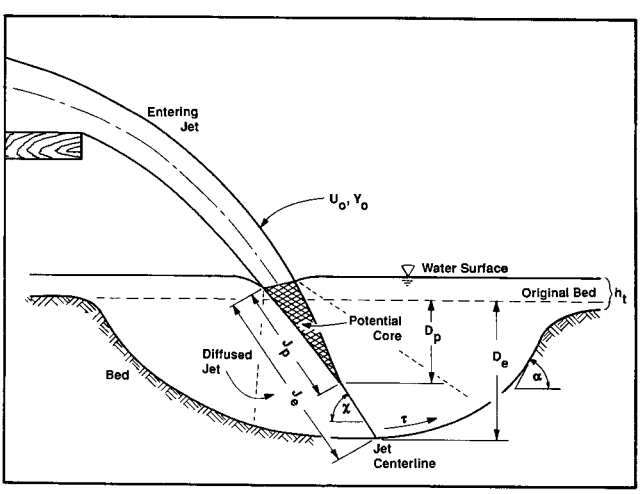

Fig. 1. Plunge pool definition sketch.
Schéma de définition de la fosse de dissipation.

The generally accepted formulation for the centerline velocity where $J > J_p$ (Rajaratnam, 1976) is:

$$\frac{U}{U_o} = C_d \sqrt{\frac{y_o}{J}}: \qquad J > J_p \tag{1}$$

where J is the distance from the origin along the centerline and the diffusion constant $C_d \approx 2.47$ is similar to the value (≈ 2.28) suggested by Albertson et al. (1950). Turbulence and non-uniform flow velocity at the jet origin influences both C_d and J_p. The length of the potential core can be simply obtained by solving equation (1) when $U = U_o$ at $J = J_p$:

$$J_p = C_d^2 y_o \tag{2}$$

Impinging jets, deflected by a flat impervious boundary, were analyzed by Beltaos (1972, 1974). His results (Beltaos 1976a, 1976b; Beltaos and Rajaratnam 1973, 1974, and 1977) identify three distinct regions in an impinging jet. The flow is analogous to a free jet for some distance from the origin and analogous to a wall jet beyond some lateral distance along the boundary from impingement. Between these regions, the boundary forces the jet to deflect causing the velocity streamlines to curve and an excess static pressure to develop. Beltaos defined the impingement region as the region in which streamlines resemble neither a free nor wall jet. His expressions for the maximum velocity in the free jet and impingement regions can be converted to the form of equation (2) in which only the value of the coefficient C_d varies. These values are 2.50 in the free jet region and 2.72 in the impingement region suggesting that an impervious boundary increases the effective diffusion constant.

Robinson (1989a,b) measured shear stress distributions along a flat impervious boundary produced by an impinging jet beneath a free overfall. His data shows that time averaged shear stress can be as much as one order of magnitude less than the maximum instantaneous value suggesting that turbulence cannot be neglected when considering jet scour.

2.1 *Equilibrium scour depth*

Most studies on the equilibrium scour depth from impinging jets have taken a rather empirical approach. Mason and Arumugam (1985) combined many previous model and prototype data sets including Cola, 1965; Hartung and Häusler, 1973; Martins, 1973, 1975 and concluded that none of the existing equations accurately predict equilibrium scour depth over the combined data sets. They attributed this to the limited dependent variables and wide range of hydraulic conditions existing in this data set.

Other researchers have used jet hydraulics to explain laboratory observations. Kobus et al. (1979) described two distinct scour hole shapes, also noted by Akashi and Saitou (1986), dependent on a dimensionless porosity factor and particle Reynolds number. Rajaratnam (1981, 1982) expanded Rajaratnam's and Beltaos' previous studies on impervious impingement to erodible beds. Mih and Kabir (1983) used Rajaratnam's analysis to study the interaction between natural streambed jet scour and armoring.

Chee and Yuen (1985) used dimensional analysis and previous relations of Beltaos (1976a) to predict the equilibrium scour depth from a large data set of jet impingement on gravel beds at various angles from 45° to 90°. They concluded that the jet impinges on the bed at the same angle as upon tailwater entry and suggested the following relationship for equilibrium scour depth D_e measured from the original unscoured bed:

$$D_e = J_e \sin\chi - h_t \tag{3}$$

where J_e is the jet centerline length from tailwater entry to bed impingement at equilibrium, h_t is the tailwater depth above the original unscoured bed and χ is the jet impingement angle.
Bormann (1988) and Bormann and Julien (1991) provide a unifying methodology for prediction of non-cohesive equilibrium scour depth produced by a large variety of jet configurations from deeply submerged wall jets to impinging unsubmerged jets by relating the jet hydrodynamic forces to particle stability. This is the explicit approach taken by Chee and Yuen (1985) and implicitly taken by Rajaratnam (1981, 1982) but Bormann generalizes and adds an approach similar to Stevens and Simons (1971) to account for particle stability on a sloping bed. He used equation (3) to determine D_e after the equilibrium scour length J_e is determined from the following:

$$J_e = \left[\frac{\varrho \sin\phi}{2g(\varrho_s - \varrho)\sin(\phi + \alpha)}\right]^{0.8} \frac{C_d^2 U_o^{1.6} y_o^{0.6}}{d_{50}^{0.4}} \tag{4}$$

where ϱ and ϱ_s are fluid and particle mass densities respectively, d_{50} is the mean sediment size, g the gravitational acceleration, α is the average angle of the scour hole and ϕ is the sediment angle of repose. Bormann's analysis shows relatively good agreement between measured and predicted equilibrium scour length J_e. Comparatively more scatter is obtained for predicted versus measured equilibrium scour depth D_e because of the difficulty in determining the jet impingement angle under various flow conditions.

2.2 *Rate of scour*

Rouse (1940) first suggested that scour depth increases linearly with the log of time. This approximation assumes that the scour depth increases infinitely with time and invalidates the concept of equilibrium scour depth. Laursen (1952) convincingly argued for the concept of equilibrium scour depth using the Shields parameter threshold. At some time, however long, the scour hole will have eroded to the point that the maximum average shear stress of the diffused jet equals the critical shear stress of the given bed material. This analysis of course ignores the effect on scour of turbulent bursts, which as Robinson (1989a, b) reports may have significant magnitude.
Despite the incompatibility between the concept of equilibrium scour depth and the semi-logarithmic time relationship, this rate model has also been used by Breusers (1967), Rajaratnam (1981), and Popova and Vedeneyev (1988). These predictive equations generally underestimate the scour depth at very short times and this discrepancy exists for a longer period of time for larger scale models. Additionally, scatter about the regression equations tends to increase at the longest measured times, possibly because at long times the magnitude of applied bed shear stress is approaching the critical shear stress of the bed material and turbulent fluctuations become the dominant erosive force.
Blaisdell et al. (1981) regressed an identical scour depth with time data set using semi-log, log-log and hyperbolic functions. The semi-logarithmic equation gave the poorest fit even when early data points are removed. The hyperbolic function has a computable equilibrium scour depth and gives the best fit, however the nature of this equation requires determination of a focal point which must be determined by trial and error. It is interesting to note that the predicted equilibrium depth using the hyperbolic function is reached 30,644 years after scour initiation, indicating that equilibrium scour depth may be reached only after extremely long times.

3 Analytical development

This section provides the analytical development for:
1. the evaluation of the equilibrium scour depth;
2. the time evolution of scour.

The development is quite general encompassing most previously published methods for equilibrium scour depth. It is applicable for any time during the scour process, and a variety of jet configurations and bed materials including cohesive particles.

3.1 *Equilibrium scour depth* D_e

The maximum shear stress acting upon the bed in the impingement region τ can be related to the maximum velocity in the impingement region U by introducing a coefficient of friction C_f.

$$\tau = C_f \varrho U^2 \tag{5}$$

Combining equations (1) and (5), with consideration of equation (2), gives the maximum applied bed shear stress τ, which within the potential core is constant at $\tau = \tau_o$:

$$\tau_o = C_f \varrho U_o^2 \qquad J \leq J_p \tag{6}$$

$$\tau = C_d^2 C_f \varrho U_o^2 \frac{y_o}{J} \qquad J > J_p \tag{7}$$

where J is the distance along the jet centerline from tailwater impingement to the eroding bed, J_p is the length of the jet potential core, U_o and y_o are the jet velocity and jet thickness at tailwater impingement, C_d is the diffusion coefficient and C_f is the friction coefficient.

The applied shear stress is a maximum when the eroding bed is within the potential core (equation (6)). When the bed is eroded beyond the depth of the potential core, the applied shear stress τ is inversely proportional to J (equation (7)) and decreases until τ approaches the critical shear stress for the bed material τ_c. This condition describes the equilibrium scour depth D_e. Equations (3) and (7) can be combined for the equilibrium scour depth when $\tau = \tau_c$, $J = J_e$ and the depth of tailwater is insignificant ($h_t \ll D_e$).

$$D_e = \frac{C_d^2 C_f \varrho U_o^2 y_o}{\tau_c} \sin\chi \tag{8}$$

This equation is a general expression for the equilibrium scour depth produced by an impinging jet for any jet configuration and bed material.

3.2 *Rate of scour*

The sediment detachment rate per unit area E (mass/time/area) at the point of maximum scour can be determined from sediment continuity as the product of sediment bulk density B (mass of solids/total volume) times change in scour depth D with time t. An excess shear equation is often used to determine the detachment rate in erosion models (Foster et al., 1977). Equating sediment continuity with the excess shear equation yields:

$$E = B \frac{\partial D}{\partial t} = \varkappa(\tau - \tau_c)^{\xi} \tag{9}$$

where $\varkappa$ and ξ are experimentally determined constants. Within the potential core, $\tau = \tau_o$, the change in scour depth D with time is given from equations (6) and (9):

$$\frac{dD}{dt} = \frac{\varkappa}{B}(C_f \varrho U_o^2 - \tau_c)^{\xi} \tag{10}$$

Integration of equation (10) from $t = 0$ to $t = T_p$ yields the time T_p at which the bed elevation is just at the tip of the potential core. The depth D_p corresponding to T_p is obtained by combining equations (2) and (3), with the assumption that the tailwater depth is insignificant ($h_t \ll D_e$).

$$T_p = \frac{BD_p}{\varkappa(C_f \varrho U_o^2 - \tau_c)^{\xi}} \tag{11}$$

$$D_p = C_d^2 y_o \sin\chi \tag{12}$$

Equations (10–12) show that scour depth D increases linearly with time t as long as the bed is within the potential core, $D \leq D_p$. Beyond the potential core, $\tau_c < \tau < \tau_o$, equation (7) shows that the maximum shear stress decreases with J due to increasing erosion of the scour hole. From equations (3), (6), (7), (9) and (12) and assuming $h_t \ll D_e$, a non-linear ordinary differential equation is obtained:

$$\frac{dD}{dt} = \frac{\varkappa}{B}\left[\frac{\tau_o D_p}{D} - \tau_c\right]^{\xi} \tag{13}$$

The equilibrium scour depth D_e is obtained when the time change in scour depth is zero, thus from equation (13):

$$\frac{D_e}{D_p} = \frac{\tau_o}{\tau_c} \tag{14}$$

Introduction of a dimensionless depth $D^* = D/D_e$, and dimensionless time $T^* = t/T_r$ where T_r is a reference time formulated from hydraulic and sediment parameters:

$$T_r = \frac{BD_e}{\varkappa\tau_o^{\xi}}\left(\frac{D_e}{D_p}\right)^{\xi} = \frac{BD_e}{\varkappa\tau_c^{\xi}} \tag{15}$$

the variable separable non-linear ordinary differential equation (13) transforms to:

$$\int_{D_p^*}^{D^*} \frac{D^{*\xi}}{(1-D^*)^{\xi}}\,dD^* = \int_{T_p^*}^{T^*} dT^* \tag{16}$$

where $D_p^* = D_p/D_e$ and $T_p^* = T_p/T_r$.

There is debate as to the proper value of the sediment detachment exponent ξ. The value of 1.5, as originally proposed by Foster et al. (1977), is derived from non-cohesive sediment transport equations, but more recent studies on cohesive soil detachment (Nearing et al., 1989; Hanson, 1989; Stein and Julien, 1991) have suggested or measured a value of 1.0. Solutions to equation (16) for $D^* \geq D_p^*$ and values of $\xi = 1, 1.5$, and for comparison as an upper limit $\xi = 2$, are provided in equations (17a), (17b) and (17c), respectively.

$$T^* - T_p^* = -D^* - \ln(1-D^*)\Big|_{D_p^*}^{D^*} \tag{17a}$$

$$T^* - T_p^* = (D^* - D^{*2})^{0.5}\left(1 - \frac{2}{D^* - 1}\right) - 1.5 \arcsin(2D^* - 1)\Big|_{D_p^*}^{D^*} \tag{17b}$$

$$T^* - T_p^* = D^* - 1 + \frac{1}{1 - D^*} + 2\ln(1 - D^*)\Big|_{D_p^*}^{D^*} \tag{17c}$$

The normalized time T_p^* corresponding to the depth of potential core scour is shown to be a function of depth or shear stress by combining equations (11), (14) and (15):

$$T_p^* = D_p^*\left(\frac{D_p^*}{1 - D_p^*}\right)^{\xi} = \frac{\tau_c}{\tau_o}\left(\frac{\tau_c}{\tau_o - \tau_c}\right)^{\xi} \tag{18}$$

This equation when combined with equation (17) provides a relation between maximum scour depth and time applicable when the bed is beyond the potential core.
The equivalent dimensionless form within the potential core ($T^* \leq T_p^*$) is obtained by combining equations (10), (14) and (15):

$$T^* = D^*\left(\frac{D_p^*}{1 - D_p^*}\right)^{\xi} \quad \text{when} \quad D^* \leq D_p^* \tag{19}$$

Solutions to equations (17), (18) and (19) are plotted, in terms of D^* versus T^*, in Fig. 2 for $\xi = 1$, 1.5 and 2 and $D_p^* = 0.0$, 0.4 and 0.8 respectively. Note that values of $D^* \leq D_p^*$ correspond to depths within the potential core and equation (19) applies. Values of $D^* \geq D_p^*$ correspond to depths beyond the potential core and equations (17) and (18) apply. As readily seen from Fig. 2 scour depth increases rapidly initially, especially for large values of D_p^*. Scour rate decreases rapidly as the equilibrium scour depth is approached and depth asymptotically approaches the equilibrium scour depth. For any value of D_p^* and ξ, scour depth is within 95% of the equilibrium depth when $T^* \geq 10$ and within 99.9% when $T^* \geq 100$. For many input values these percentages are reached considerably earlier in the scour process. Also note that at no time during the scour process does depth increase with the log of time, however this approximation is valid at intermediate times which may explain its use in many previous studies.

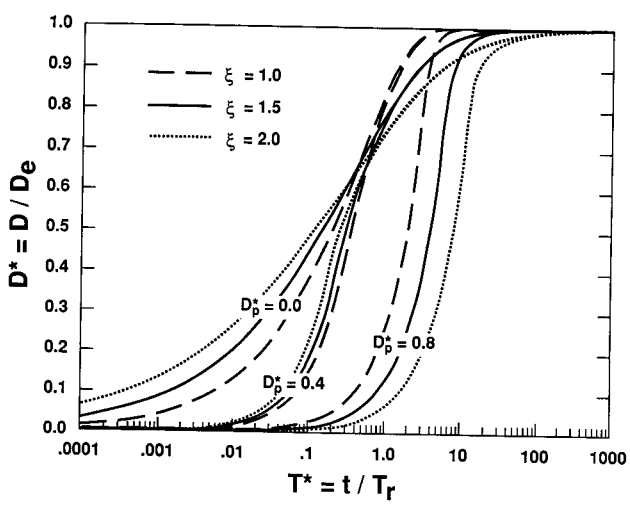

Fig. 2. Theoretical scour depth versus time.
Profondeur d'affouillement théorique en fonction du temps.

4 Laboratory experiments

Several laboratory experiments were conducted in the Hydraulics Laboratory at Colorado State University to test the theoretical relationships developed in the previous section.

4.1 *Materials and methods*

An impinging jet, similar to that which may occur below a natural headcut, was created by a free overfall at the end of a 100.0 cm long plexiglas plate set within a 10.4 cm wide by 200.0 cm long and 33.0 cm high plexiglas flume. The flume was set at 3.7% slope for all experimental runs. Each run on a given bed material represents a unique jet configuration determined by varying either the discharge or drop height between the plexiglas plate and erodible bed test section. Discharge was controlled by a pressure regulator and measured by a turbine meter in the non-recirculating flume supply line. Drop height was controlled by an exit plate set downstream from the 40.0 cm test section. Tailwater depth was therefore the normal flow depth for the given downstream hydraulic condition.

Two-dimensional scour profiles from a jet impinging on three different saturated bed materials were measured in the flume at sequential times throughout the scour process. Eight runs on a coarse sand with a mean diameter d_{50} of 1.5 mm, six runs on a fine sand $d_{50} = 0.15$ mm, and ten runs on a cohesive soil $d_{50} = 0.045$ mm were conducted. The particle size distribution of each material is given in Fig. 3. The cohesive soil is a typical agricultural soil collected from a field in eastern Colorado, USA (Norka, fine silty, mixed mesic, Aridic Argiustoll 5-9% slope). To make soil conditions as uniform as possible, and to remove large pieces of organic matter, the air dried soil was passed through a 0.420 mm sieve. This destroyed all but the natural soil's micro-aggregate structure and allowed it to retain cohesive properties upon re-wetting.

The set-up procedure for each run consisted of filling the flume test section including a volume underneath the upstream plexiglas plate with the desired bed material in 5 cm layers. The bed material was then slowly saturated from the bottom up. This method produced a uniform bulk density and water content for each bed material.

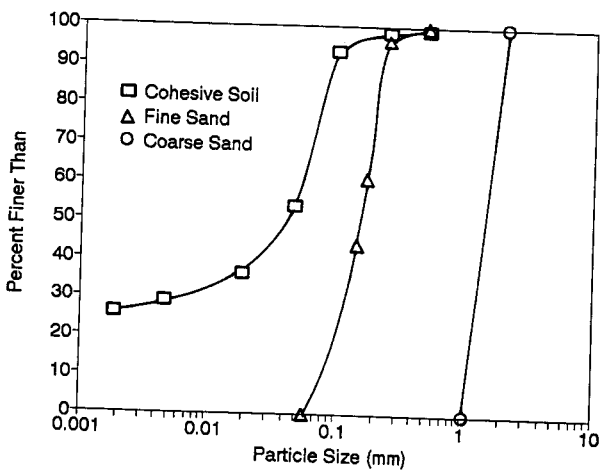

Fig. 3. Bed particle size distribution.
Granulométrie du matériau de fond.

Determining bed profile changes both quickly and accurately was critical to this study. A point gauge was used to determine initial, selected intermediate and final bed profiles. It is impossible to measure the entire profile at any instant during the run by this method, therefore a photographic technique was developed. A translucent acetate imprinted with a millimeter grid was adhered to the flume sidewall. An approximate 35 × 22 cm area of the test section was photographed through the acetate at intervals ranging from 5 sec. initially to 10 min. at the longest times, depending on the rate of profile change. Typically 30 to 40 profiles were taken per run. Accurate bed and water surface profiles, taken at virtually instantaneous selected times by this photographic technique, were digitized to store the x, y, t coordinates of the bed profiles. These coordinates were used to determine bed profiles, volume of eroded material, and maximum depth of scour at instantaneous times. Details of the experimental set-up, data collection and run specifics are given in Stein (1990).

4.2 *Results and discussion*

Typical scour profiles determined from the photographic technique for the cohesive soil (Run 8) and fine sand $d_{50} = 0.15$ mm (Run 26) over a period of approximately 2.5 hours are shown in Figs. 4a and 4b respectively. As expected, the scour rate is most rapid initially and decreases with time.

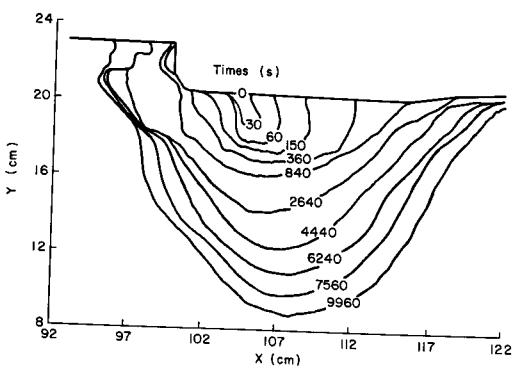

Fig. 4a.
Cohesive soil scour profiles versus time.
Profiles d'affouillement en sol cohésif en fonction du temps.

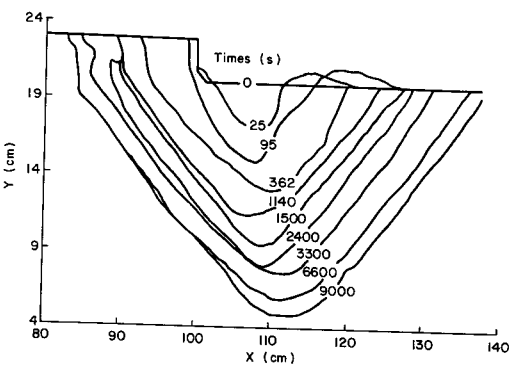

Fig. 4b.
Fine sand scour profiles versus time.
Profils d'affouillement avec du sable fin en fonction du temps.

The profile shape for all runs is approximately symmetrical about the maximum depth of scour with a slight skewness in the downstream direction. Maximum depth of scour is in the vicinity of the calculated centerline of the impinging jet, but unlike results of Chee and Yuen (1985) this maximum is consistently shifted in the upstream direction.

4.2.1 Equilibrium scour depth

Virtually all theoretically guided predictive equations for equilibrium scour depth can be simplified to equation (8). The validity of this equation was tested using the three bed materials. Bormann's method (equations (3) and (4)) was used without modification for non-cohesive sands (Runs 14–21, $d_{50} = 1.5$ mm, $\phi = 34°$; Runs 22–27, $d_{50} = 0.15$ mm, $\phi = 25°$) while equation (8) with

$\tau_c = 0.32$ Pascal was used for the cohesive bed material (Runs 1–13). This value was determined from an independent set of experiments as reported by Stein and Julien, (1991). A value of 2.6 was taken for the diffusion constant C_d. This value is higher than used by Bormann (1.8–2.3) but is lower than that given by Beltaos (2.72) for diffusion in the impingement region. Bormann's experiments often had a poorly defined jet and Beltaos' were for a plane, impervious boundary. The jet in the present experiments was well defined but boundaries are neither plane (except for $t = 0$) nor impervious. The coefficient of friction was determined from a Blasius flow assumption $C_f = (0.22/8)(q/\nu)^{-0.25}$ where q is unit discharge and ν is the kinematic viscosity.

The various parameters needed to determine the predicted equilibrium scour depth D_e from equations (3) and (4) or (8), the time T_M at which the run was terminated and the corresponding maximum measured depth D_{eM} are given in Table 1. All runs were terminated after a maximum 2.75 hr and for several runs this time was not sufficiently long for the equilibrium scour depth to be reached. A comparison between measured and predicted equilibrium scour depths should include this time factor when appropriate. Therefore, the expected equilibrium depth was adjusted D_{eP} to correspond to the measured time T_M using the appropriate formulation of equation (17) determined from scour rate data as detailed in the following section. This adjustment was most necessary for the largest equilibrium depths on the cohesive soil runs. The D^* value corresponding to D_{eP} (D_{eP}/D_e) varied from 0.27 to 0.88, 0.82 to 0.92 and 0.98 to 1.00 for cohesive soil, fine sand and coarse sand runs respectively. The adjusted equilibrium depth D_{eP} is compared to the measured depth D_{eM} in Fig. 5. These values are also given in Table 1. As can be seen from Fig. 5 almost all measured maximum depths are within 20% of the expected maximum depth, a considerable improvement over most previously published correlations.

Table 1. Experimental values of ultimate scour depth parameters
Valeurs expérimentales des paramètres caractérisant la profondeur limite d'affouillement

Run	D_h (mm)	q ($m^3/s \cdot m$)	U_o (m/s)	y_o (mm)	χ (o)	D_e (mm)	T_M (s)	D_{eP} (mm)	D_{eM} (mm)
13	10	0.00157	0.68	2.3	41	68	7200	60	77
12	10	0.00489	0.93	5.2	28	159	6000	101	112
7	20	0.00154	0.81	1.9	51	94	6240	72	81
3-4	20	0.00225	0.87	2.6	46	125	8340	98	84
11	20	0.00346	0.95	3.6	41	173	9000	123	130
6	20	0.00450	1.01	4.4	38	211	6000	122	122
8	40	0.00172	1.04	1.7	59	145	9960	113	119
1	40	0.00230	1.07	2.1	56	180	745	49	51
10	40	0.00354	1.14	3.1	51	249	9000	157	128
9	40	0.00458	1.19	3.8	48	302	4080	136	142
21	20	0.00162	0.82	2.0	50	47	9000	47	45
20	20	0.00257	0.89	2.9	45	63	4080	62	58
19	20	0.00347	0.95	3.7	41	76	1800	75	73
18	20	0.00493	1.04	4.8	37	96	1800	94	82
14	40	0.00168	1.03	1.6	59	68	1800	67	38
15	40	0.00235	1.08	2.2	55	83	1800	81	57
16	40	0.00353	1.14	3.1	51	106	1800	104	74
17	40	0.00480	1.20	4.0	47	129	5220	129	97
22	20	0.00166	0.82	2.0	50	99	9000	91	103
23	20	0.00232	0.87	2.7	46	122	9000	112	132
24	20	0.00349	0.95	3.7	41	161	9000	143	163
27	40	0.00175	1.04	1.7	59	140	9000	115	134
26	40	0.00242	1.08	2.2	55	172	9000	151	162
25	40	0.00337	1.13	3.0	51	212	9000	193	175

Table 2. Experimental values of scour depth evolution parameters
Valeurs expérimentales des paramètres caractérisant l'évolution de la profondeur d'affouillement

Run	B (kg/m^3)	D_p (m)	D_e (m)	D_p^*	τ_0 (Pa)	$\varkappa$ [1]	ξ	T_r (s)
13	1290	0.010	0.068	0.15	2.21	0.04	1.0	6615
12	1290	0.017	0.159	0.11	3.12	0.04	1.0	15509
7	1290	0.010	0.094	0.11	3.14	0.04	1.0	9220
3-4	1290	0.013	0.125	0.10	3.27	0.04	1.0	12253
11	1290	0.016	0.173	0.09	3.52	0.04	1.0	16921
6	1290	0.019	0.211	0.09	3.74	0.04	1.0	20607
8	1290	0.010	0.145	0.07	4.99	0.04	1.0	14167
1-2	1290	0.012	0.180	0.07	4.97	0.04	1.0	17617
10	1290	0.016	0.249	0.07	5.06	0.04	1.0	24343
9	1290	0.019	0.302	0.06	5.18	0.04	1.0	29531
21	1350	0.010	0.047	0.22	3.15	0.98	1.5	115
20	1350	0.014	0.063	0.22	3.33	0.98	1.5	140
19	1350	0.016	0.076	0.21	3.52	0.98	1.5	161
18	1350	0.019	0.096	0.20	3.83	0.98	1.5	192
14	1350	0.009	0.068	0.14	4.99	0.98	1.5	163
15	1350	0.012	0.083	0.15	4.97	0.98	1.5	184
16	1350	0.016	0.106	0.15	5.06	0.98	1.5	216
17	1350	0.020	0.129	0.15	5.21	0.98	1.5	247
22	1670	0.010	0.099	0.11	3.16	0.30	1.5	2837
23	1670	0.013	0.122	0.11	3.28	0.30	1.5	3354
24	1670	0.016	0.161	0.10	3.53	0.30	1.5	4172
27	1670	0.010	0.140	0.07	4.99	0.30	1.5	3858
26	1670	0.012	0.172	0.07	4.97	0.30	1.5	4433
25	1670	0.016	0.212	0.07	5.04	0.30	1.5	5155

[1] Units dependent on value of ξ; s/m if $\xi = 1.0$, $s^2/m^{0.5} \cdot kg^{0.5}$ if $\xi = 1.5$

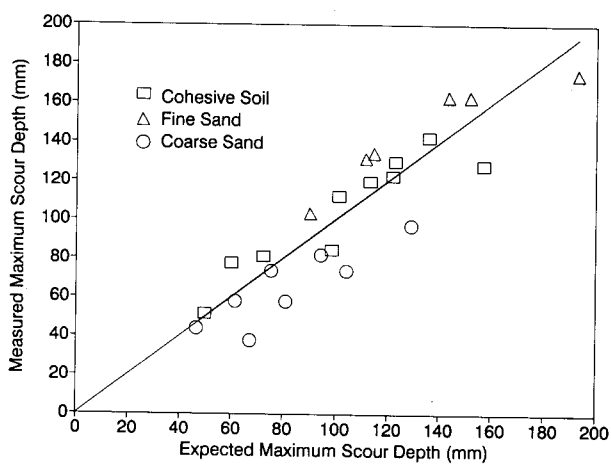

Fig. 5. Predicted versus measured equilibrium scour depth.
Profondeur d'affouillement à l'équilibre. Comparaison calcul-mesures.

4.2.2 Rate of scour

The applicability of equations (17), (18) and (19) for scour depth increase was tested using the same runs as described for equilibrium depth. The depth of potential core scour $D_p^* = D_p/D_e$ varies slightly in the experiments from 0.06 to 0.15 for cohesive soil, 0.07 to 0.11 for fine sand and 0.14 to 0.22 for the coarse sand. As seen in Fig. 2, D_p^* strongly influences scour rate, but within the small experimental range is insignificant. The raw data were normalized using the reference time T_r calculated assuming $\xi = 1$, 1.5 and 2. The parameter $\varkappa$ was adjusted for each bed material and ξ value to provide the best fit between theory and experimental results. Plots of the measured increase in normalized scour depth D^* with normalized time T^* for ten cohesive soil runs, six fine sand runs and seven coarse sand runs are compared with predicted values in Figs. 6, 7 and 8, respectively. The sand runs have the best fit when $\xi = 1.5$ and $\varkappa = 0.98$ ($s^2 \cdot kg^{-0.5} \cdot m^{-0.5}$) for the

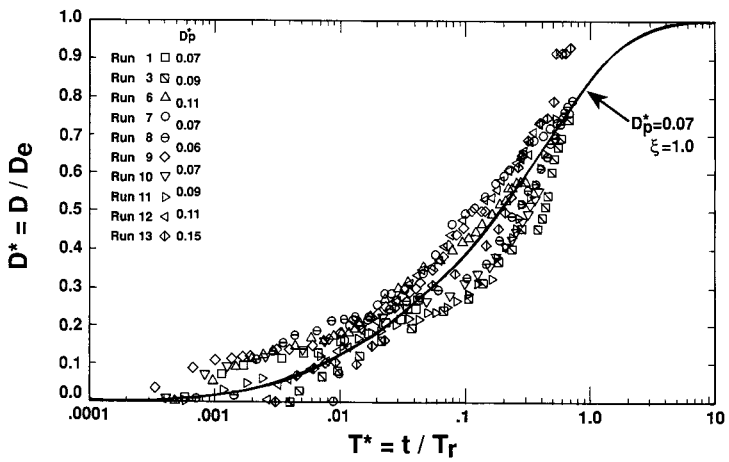

Fig. 6. Predicted versus measured scour depth evolution; cohesive soil.
Evolution de la profondeur d'affouillement; sol cohésif. Comparaison calcul-mesures.

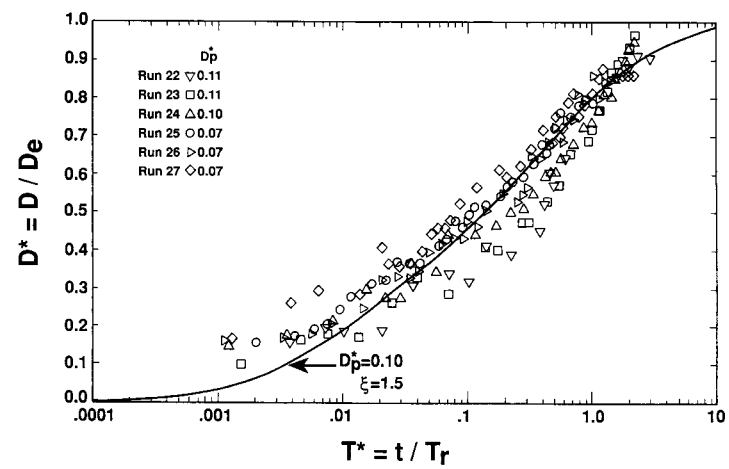

Fig. 7. Predicted versus measured scour depth eveolution; fine sand.
Evolution de la profondeur d'affouillement; sable fin. Comparaison calcul-mesures.

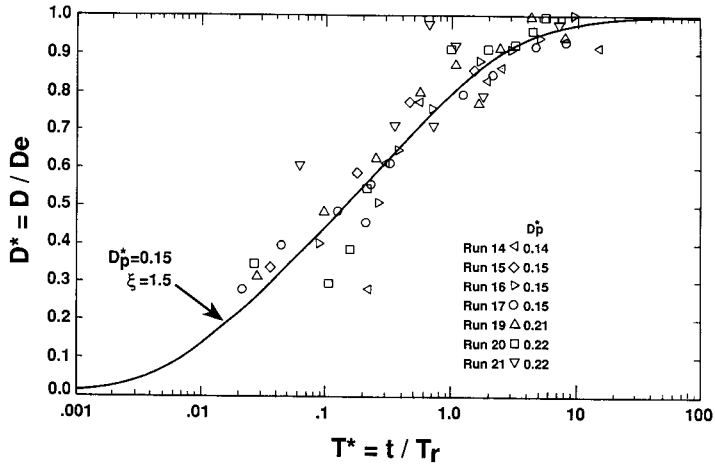

Fig. 8. Predicted versus measured scour depth evelution; coarse sand.
Evolution de la profondeur d'affouillement; sable grossier. Comparaison calcul-mesures.

coarse sand and 0.30 for the fine sand. The cohesive soil runs have the best fit with $\xi = 1.0$ and $x = 0.04$ (s · m^{-1}). As discussed in Stein and Julien (1991), these data support previously proposed or measured values of the experimental constant ξ. The change in measured scour depth is not linear with the log of time for any bed material or value of the experimental constants, x and ξ. The present analysis with the proper choice of constants is a marked improvement over the semi-logarithmic linear model.

5 Conclusions

The change in maximum scour depth with time produced by an impinging jet proceeds at a rate dependent on the position of the bed relative to the jet origin, which in general corresponds to the tailwater elevation, but in this study, with an extremely shallow tailwater depth, corresponds to the original bed elevation. The rate can be analytically determined by relating the maximum velocity of a diffusing jet at a specific time with the generally accepted excess shear sediment detachment equation while considering sediment continuity at the eroding bed's surface. Initially during the scour process, while the bed surface is within the jet's potential core ($D^* \leq D_p^*$), the rate is constant and given by equation (10). Thereafter ($D^* \geq D_p^*$), the scour rate decreases with time as given by equation (13). The scour depth asymptotically approaches an equilibrium depth D_e calculated from equation (8). Using the proper normalizing parameters $D^* = D/D_e$ and $T^* = t/T_r$, with T_r from equation (15), the rate of scour can be calculated for any bed material, jet configuration and time within the scour process using equations (17-19). A graphical representation of these equations, as shown in Fig. 2, reveals that, regardless of input parameters, scour depth is within 95% of the equilibrium depth for $T^* \geq 10$. This condition is reached sooner for a larger critical shear stress and/or a smaller jet.

The validity of the developed equations has been tested in the laboratory with non-cohesive and cohesive bed materials. Agreement between measured and predicted equilibrium scour depths is generally within 20% as shown in Fig. 5. This agreement is generally better than previously

published results for non-cohesive material and has the advantage of being equally applicable to cohesive bed materials. Correlation between the measured and predicted scour rate is equally good with the proper choice of the excess shear sediment detachment parameters, as shown in Figs. 6, 7 and 8. The results indicate that the value of the sediment detachment exponent ξ is 1.5 for non-cohesive sand and 1.0 for cohesive soil and thus supports previously published conclusions. The usage of an impinging jet holds promise as an improved method for the determination of all experimental parameters of the excess shear sediment detachment equation.

Acknowledgements

This study has been primarily funded by the USDA-ARS Hydro-Ecosystems Research Group. Additional support is provided by the ARO Center for Geosciences at Colorado State University (Grant ARO/DAAL 03-86-K-0175) and the Montana State Agricultural Experiment Station (Paper no. J-2703). Our appreciation goes to all groups.

List of symbols

B soil bulk density
C_d diffusion constant of a jet
C_f coefficient of friction
d_{50} mean sediment size
D maximum depth of jet scour at a given time t
D^* normalized maximum scour depth (D/D_e)
D_e equilibrium depth of jet scour
D_{eM} measured scour depth at time T_M
D_{eP} predicted scour depth at time T_M
D_h drop height of the headcut
D_p depth of scour corresponding to potential core tip
D_p^* normalized depth of potential core tip (D_p/D_e)
E sediment detachment rate per unit area
g gravitational acceleration
h_t depth of tailwater
J distance along a jet centerline
J_e distance along a jet centerline to impingement at equilibrium
J_p length of a jet potential core
q unit flow discharge
t time
T^* normalized time (t/T_r)
T_M time at which the maximum scour depth was measured
T_p time corresponding to potential core scour depth D_p
T_p^* normalized time (T_p/T_r)
T_r reference time
U maximum diffused jet velocity
U_o initial jet velocity
y_o initial jet thickness
$\varkappa, \xi$ constants of sediment detachment equation

α average angle of scour hole boundary
ν fluid kinematic viscosity
ϱ fluid density
ϱ_s particle density
τ_c critical shear stress for erosion initiation
τ shear stress in the impingement region
τ_o shear stress in the potential core
ϕ angle of repose of submerged sediment
χ jet angle at tailwater impingement

References

1. ALBERTSON, M. L., DAI, Y. B., JOHNSON, R. A. and ROUSE, H. (1950), Diffusion of Submerged Jets, Trans. ASCE 115, pp. 639–697.
2. AKASHI, N. and SAITOU, T. (1986), Influence of Water Surface on Scour From a Vertical Submerged Jet, J. of Hydroscience and Hydr. Engr. 4(2) pp. 55–69.
3. BELTAOS, S. (1972), Normal Impingement of Plane Turbulent Jets on Sooth Walls, M.S. Thesis, University of Alberta, Edmonton, Alberta, Canada.
4. BELTAOS, S. (1974), Turbulent Impinging Jets, Ph.D. Dissertation, University of Alberta, Edmonton, Alberta, Canada.
5. BELTAOS, S. (1976a), Oblique Impingement of Plane Turbulent Jets, J. Hydr. Div., ASCE 102(HY9), pp. 1177–1192.
6. BELTAOS, S. (1976b), Oblique Impingement of Circular Turbulent Jets, J. Hydr. Res. 14(1), pp. 17–36.
7. BELTAOS, S. and RAJARATNAM, N. (1973), Plane Turbulent Impinging Jets, J. Hydr. Res. 11(1), pp. 29–59.
8. BELTAOS, S. and RAJARATNAM, N. (1974), Impinging Circular Turbulent Jets, J. Hydr. Div., ASCE 100(HY10), pp. 1313–1328.
9. BELTAOS, S. and RAJARATNAM, N. (1977), Impingement of Axisymmetric Developing Jets, J. Hydr. Res. 15(4), pp. 311–325.
10. BLAISDELL, F. W., ANDERSON, C. L. and HEBAUS, G. G. (1981), Ultimate Dimensions of Local Scour, J. Hydr. Div., ASCE 107(HY3), pp. 327–337.
11. BORMANN, N. E. (1988), Equilibrium Local Scour Depth Downstream of Grade Control Structures, Ph.D. Dissertation, Colorado State University, Fort Collins, Co.
12. BORMANN, N. E. and JULIEN, P. Y. (1991), Scour Downstream of Grade Control Structures, J. Hydr Engr. 117(5), pp. 579–594.
13. BREUSERS, H. N. C. (1967), Time Scale of Two Dimensional Local Scour, Inter. Asso. Hydr. Res. Proc., 12th Congress, Vol. 3, pp. 275–282, Paper No. C32.
14. CHEE, S. P. and YUEN, E. M. (1985), Erosion of Unconsolidated Gravel Beds, Can. J. Civ. Engr. 12, pp. 559–566.
15. COLA, R. (1965), Energy Dissipation of a High-Velocity Vertical Jet Entering a Basin, Inter. Asso. Hydr. Res. Proc., 11th Congress, Vol. 1, Paper No. 1.52.
16. FOSTER. G. R., MEYER, L. D. and ONSTAD, C. A. (1977), An Erosion Equation Derived From Basic Erosion Principles, Trans. ASAE 20(4), pp. 678–682.
17. HANSON, G. L. (1989), Channel Erosion Study of Two Compacted Clays, Trans. ASAE 32(5), pp. 485–490.
18. HARTUNG, F. and HÄUSLER, E. (1973), Scours, Stilling Basins and Downstream Protection Under Free Overfall Jets at Dams, 11th Inter. Comm. Large Dams Trans., Vol II Q41, Paper R3, pp. 39–56.
19. KOBUS, H., LEISTER, P. and WESTRICH, B. (1979), Flow Field and Scouring Effects of Steady and Pulsating Jets Impinging on a Moveable Bed, J. Hydr. Res. 17(3), pp. 175–192.
20. LAURSEN, E. M. (1952), Observations on the Nature of Scour, Proc. 5th Hydr. Conf., University of Iowa, Iowa City, Iowa Bul. 34, pp. 179–197.
21. MARTINS, R. (1973), Contribution to the Knowledge on the Scour Action of Free Jets on Rocky River-Beds, 11th Inter. Comm. Large Dams Trans., Vol. II Q41, Paper R44, pp. 799–814.
22. MARTINS, R. (1975), Scouring of Rocky River-Beds by Free-Jet Spillways, Inter. Water Pow. Dam Constr. 27(4), pp. 152–153.
23. MASON, P. J. and ARUMUGAM, K. (1985), Free Jet Scour Below Dams and Flip Buckets, J. Hydr. Engr. 111(2), pp. 220–235.

24. MIH, W. C. and KABIR, J. (1983), Impingement of Water Jets on Nonuniform Streambed, J. Hydr. Engr. 109(4), pp. 536-548.
25. NEARING, M. A., FOSTER, G. R., LANE, L. J. and FINKNER, S. A. (1989), A Process-Based Soil Erosion Model for USDA Water Erosion Prediction Project Technology, Trans. ASAE 32(5), pp. 1587-1593.
26. POPOVA, K. S. and VEDENEYEV, Y. E. (1988), Time Variation in the Depth of Local Scour Downstream of Dams, Fluid Mech. - Soviet Res. 17(3), pp. 123-134.
27. RAJARATNAM, N. (1976), Turbulent Jets: Development in Water Science #5, Elsevier Scientific Publishing Co., Amsterdam, The Netherlands.
28. RAJARATNAM, N. (1981), Erosion by Plane Turbulent Jets. J. Hydr. Res. 19(4), pp. 339-359.
29. RAJARATNAM, N. (1982), Erosion by Unsubmerged Plane Water Jets. In: Applying Research to Hydraulic Practice, ASCE Conf., Jackson, MS, pp. 280-288.
30. ROBINSON, K. M. (1989a), Stress Distribution at an Overfall, Trans. ASAE 32(1), pp. 75-80.
31. ROBINSON, K. M. (1989b), Hydraulic Stress on an Overfall Boundary, Trans. ASAE 32(4), pp. 1269-1274.
32. ROUSE, HUNTER (1940), Criteria for Similarity in the Transportation of Sediment, Proc. 1st Hydraulic Conf., State University of Iowa, Iowa City, Iowa, pp. 33-49.
33. STEIN, O. R. (1990), Mechanics of Headcut Migration in Rills, Ph.D. Dissertation, Colorado State University, Fort Collins, CO 80523.
34. STEIN, O. R. and JULIEN, P. Y. (1991), Measurement of Rill Erosion Sediment Detachment, ASAE Paper No. 91-2086, Presented Internat. Summer Meetings, June 23-26, Albuquerque, NM, USA.
35. STEVENS M. A. and SIMONS, D. B. (1971), Stability Analysis for Coarse Granular Material. In: River Mechanics, Vol. 1, (Chap. 17), H. W. Shen (ed.), Fort Collins, CO.